

Free-space microwave-to-optical conversion via six-wave mixing in Rydberg atoms

Jingshan Han^{1,*}, Thibault Vogt^{1,2,*}, Christian Gross¹, Dieter Jaksch^{3,1}, Martin Kiffner^{1,3}, and Wenhui Li^{1,4}
Centre for Quantum Technologies, National University of Singapore, 3 Science Drive 2, Singapore 117543¹
MajuLab, CNRS-UNS-NUS-NTU International Joint Research Unit UMI 3654, Singapore 117543²
Clarendon Laboratory, University of Oxford, Parks Road, Oxford OX1 3PU, United Kingdom³ and
Department of Physics, National University of Singapore, 117542, Singapore⁴

PACS numbers: 42.50.Gy, 42.65.Ky, 32.80.Ee

Efficient methods for converting microwave and terahertz radiation into optical fields and vice versa have a tremendous potential for developing next-generation classical and quantum technologies. For example, these methods would facilitate the detection and imaging of millimeter waves with various applications in medicine, security screening and avionics [1–4]. In the quantum domain, coherent microwave-optical conversion is essential for realizing quantum hybrid systems [5] where spin systems or superconducting qubits are coupled to optical photons that can be transported with low noise in optical fibres [6]. Here we show that frequency mixing in Rydberg atoms is an efficient method for microwave-optical conversion due to the strong coupling of millimeter waves to Rydberg transitions and the long lifetime of Rydberg states. This frequency conversion works in free space, is tunable and broadband, and has the potential of reaching near-unity photon-conversion efficiency.

At the heart of any frequency converter is a physical system that simultaneously interacts with two frequency bands and provides an efficient link between them. In the case of millimeter waves and optical fields the corresponding bands are separated by several orders of magnitude, and hence the challenge is to devise a suitable platform that couples both of them strongly. In order to achieve this, schemes based on ferromagnetic magnons [7], frequency mixing in Λ -type atomic ensembles [8–11], whispering gallery resonators [12, 13] or nanomechanical oscillators [14–16] require high-quality cavities for the millimeter and optical fields that limit their bandwidth and tunability. Recently, highly excited Rydberg atoms have been identified as a promising alternative [17, 18] featuring strong atomic transitions in the optical regime as well as a quasi-continuum of strong dipole transitions in the terahertz and microwave range [19].

In this letter, we report an experimental demonstration of coherent and efficient microwave-to-optical conversion in free space via frequency mixing in Rydberg atoms. Our scheme as shown in Fig. 1 achieves efficient

conversion without the need for optical or microwave cavities due to the strong coupling of millimeter waves to Rydberg atoms. Furthermore, the long lifetime of Rydberg states allows us to make use of the phenomenon of electromagnetically induced transparency (EIT) [20], which significantly enhances the nonlinearity responsible for the conversion process [21]. This enhancement is known to result in near-unity conversion efficiencies for optical-to-optical conversion [22, 23]. Here we show that this frequency mixing mechanism can also be employed for coherent microwave-to-optical conversion, and our proof-of-principle experiment achieves a free-space conversion efficiency of 0.25% with a bandwidth of about 4 MHz. Optimized geometry and energy level configurations should enable the broadband inter-conversion of microwave and optical fields with near-unity efficiency [18]. Our results thus pave the way for future applications of microwave-optical conversion with Rydberg atoms.

Microwave-to-optical conversion is achieved with the experimental setup shown in Fig. 1a. The actual conversion medium is represented by a cloud of cold atoms interacting with four auxiliary fields P, C, A, and R. The conversion of the input microwave field M into the optical field L can be understood based on a single atom interacting with six fields, as illustrated by the atomic energy levels and the corresponding dipole-coupled transitions in Fig. 1b. Starting from the spin polarized ground state $|1\rangle$, the auxiliary fields and the microwave field M lead to the creation of a coherence between the states $|1\rangle$ and $|6\rangle$. This induces the emission of the light field L with frequency $\omega_L = \omega_P + \omega_C - \omega_A + \omega_M - \omega_R$ such that the resonant six-wave mixing loop is completed, where ω_X is the frequency of field X ($X \in \{P, R, M, C, L, A\}$). The direction of emission of field L is determined by the phase matching condition $\mathbf{k}_P + \mathbf{k}_C - \mathbf{k}_R - \mathbf{k}_L \approx 0$, where \mathbf{k}_X is the wave vector of the corresponding field. Here the wave vectors of the microwave fields are neglected since they are much smaller than those of the optical fields. Therefore, the converted light field L propagates collinearly with the input field P. Moreover, the transverse profile of the converted light field L resembles that of the auxiliary field P due to pulse matching [24, 25] as illustrated in the inset of Fig. 1a.

We experimentally demonstrate and characterize the six-wave mixing process with two measurements. First,

* These authors contributed equally to this work.

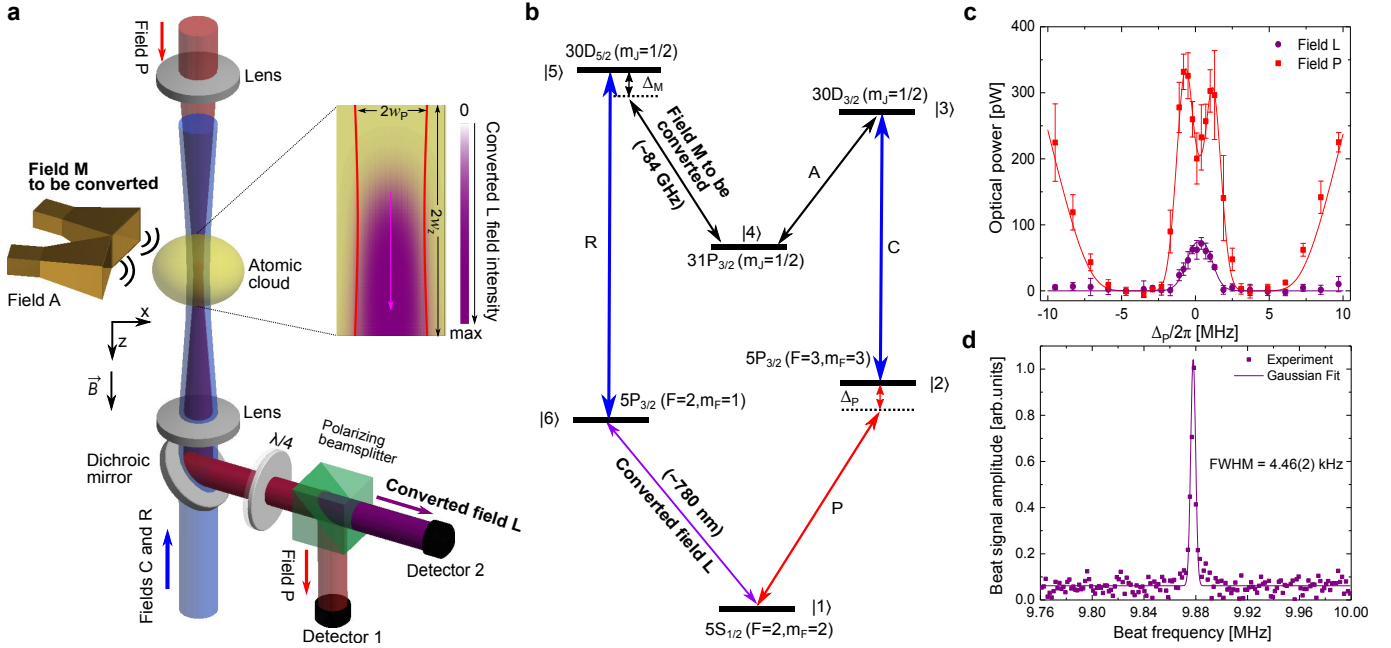


FIG. 1. **Coherent microwave-to-optical conversion.** **a**, Experimental setup. Three input auxiliary light fields P, C, and R propagate collinearly along the vertical z axis and are focused onto the center of a Gaussian-distributed atomic cloud. The quantization axis is defined by a bias magnetic field B along z . The microwave field M to be converted and the auxiliary microwave field A radiates out of two horn antennas and propagate horizontally. The converted light field L co-propagates along the same direction as the P field. Fields P and L exiting the atomic cloud are separated before being detected with avalanche photodiode detectors. The inset shows the simulated intensity and the two-dimensional beam profile of the converted light field L. w_P is the $1/e^2$ beam waist of the P field, and w_z is the $1/e^2$ radius of the atomic cloud. **b**, Schematics of relevant energy levels of a single ^{87}Rb atom coupled by six nearly-resonant electromagnetic fields. The electronic, hyperfine, and Zeeman quantum numbers for levels $|1\rangle - |6\rangle$ are given, and the vertical positions of the levels indicate how their energies are relative to each other (not to scale). Δ_P and Δ_M are the frequency detunings of the P and M fields from their respective atomic transition resonances. **c**, Spectra of the auxiliary light field P (red squares) and the converted light field L (purple circles) versus Δ_P at $\Delta_M = 0$. The solid lines are theoretically simulated spectra (see Methods). The displayed error bars correspond to a statistical confidence interval of 1σ . **d**, Spectrum of the beat signal between P and L fields at $\Delta_M = 0$ and $\Delta_P = 0$.

we scan the detuning of the P field Δ_P across the atomic resonance while all other input fields are on resonance, and simultaneously measure the powers of the transmitted field P and of the converted optical field L. The spectrum obtained from monitoring the L field possesses a pronounced peak around $\Delta_P = 0$ as denoted by the purple circles in Fig. 1c. The red squares in the same figure correspond to the P field spectrum which is used for calibration purposes. The very good agreement of the experimental spectra with numerical simulations based on Maxwell-Bloch equations (see Methods) strongly supports the conversion mechanism given above. In a second experiment, we perform a beat measurement to investigate the coherence properties of the converted light field. For this, we shift the frequency of the field P and measure the optical beat note with the converted field L (see Methods). As shown in Fig. 1d, we obtain a single narrow peak with a spectral width of 4.46(2) kHz, which indicates the high degree of coherence of the converted light. Moreover, the observed beat note frequency con-

firms that the frequency of the converted field L is indeed determined by the resonance condition for the six-wave mixing process. These measurements firmly establish the microwave-to-optical conversion scheme.

Next we characterize how the conversion process depends on the intensity and frequency of the microwave field M, while all auxiliary fields are kept on resonance and at constant intensity. We first vary its intensity I_M with the microwave detuning $\Delta_M = 0$. We find that the power of the converted field L steadily increases with increasing intensity I_M as shown in Fig. 2a. The experimental data are generally in good agreement with theoretical predictions, while the small deviations for low intensities are subject to further investigation. We note that the measured output power at $I_M \approx 44 \text{ pW/mm}^2$ corresponds to a peak intensity of the L field of $I_L \approx 67 \text{ nW/mm}^2$, which is more than three orders of magnitude larger than the microwave input intensity I_M . Second, we record the power of the converted field L as a function of the microwave detuning Δ_M for various in-

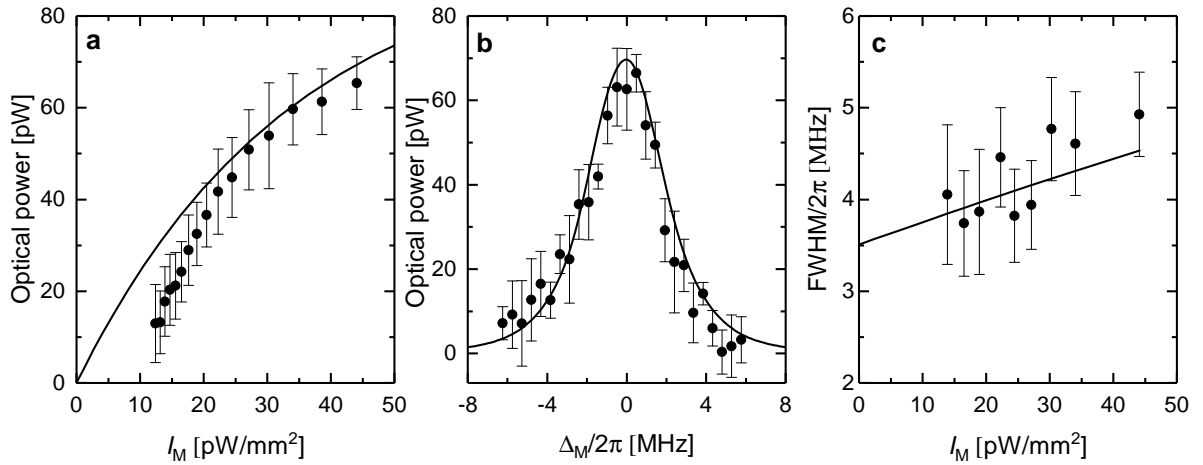


FIG. 2. **Broadband conversion.** **a**, Power of the converted light field L at $\Delta_M = 0$ and $\Delta_P = 0$ versus the M field intensity I_M . **b**, Microwave spectrum of the converted light field L. The powers of the converted light field L are plotted versus Δ_M at $I_M = 44$ pW/mm² and $\Delta_P = 0$. **c**, Full width at half maximum (FWHM) versus I_M . The FWHM are extracted by fitting a Gaussian distribution to the microwave spectra. The black circles are experimental data, while the solid lines are the corresponding theoretically simulated curves. The displayed error bars in **a** and **b** correspond to a statistical confidence interval of 1σ , and the ones in **c** indicate the errors from fitting.

tensities I_M . The spectra are bell-shaped and centered at $\Delta_M = 0$ (Fig. 2b). To investigate the bandwidth of our conversion scheme, we extract the full width at half maximum of the microwave spectra and plot them as a function of the intensity I_M in Fig. 2c. The bandwidth is of the order of a few MHz, and has a very slow linear dependence over a large range of microwave intensities. This large conversion bandwidth is one of the main advantages of our scheme and is essential for converting short pulses.

An important feature of our scheme is that the power of the converted light and hence the conversion efficiency can be enhanced by increasing the optical depth of the atomic cloud along the z direction. This is shown in Fig. 3, where the output power of the converted field L is measured as a function of the optical depth $D_P \propto n_0 w_z$, where n_0 is the peak atomic density and w_z is the $1/e^2$ radius of the atomic cloud. The experimental results (black circles) are in good agreement with the theoretical curve (black solid line) up to $D_P \approx 16$, which is the highest optical depth achievable with the current experimental setup. The theoretical curve in Fig. 3 suggests that the converted light power can be further increased until it saturates at $D_P \approx 30$. This result can be understood as follows. We find that the interaction between an atom with a level scheme as shown in Fig. 1b and six resonant fields exhibits a so-called dark state $|D\rangle$ [26] (see Supplementary Information). As the P field propagates along the z direction, the build-up of the converted light (see inset in Fig. 1a) increases the population of this state. Since atoms in state $|D\rangle$ are decoupled from the light fields, the generation of field L saturates if all the atoms

are trapped in this state, which happens for the parameters of Fig. 3 at $D_P \approx 30$.

A critical benchmark for any converter is the conversion efficiency. To evaluate the photon conversion efficiency in our setup, we consider the cylindrical volume \mathcal{V} of the atomic cloud that overlaps with all six fields and has the dimensions of $\sim 2w_P$ in diameter and of $\sim 2w_z$ in length (see Fig. 1a). Hence we calculate the efficiency as $\eta = \eta_0 \times S_L/S_M$, where $\eta_0 = E_L/E_M$ is the ratio of the photon fluxes per unit area (photon irradiances) of fields L and M, and $S_L = \pi w_P^2$ and $S_M = 4w_P w_z$ are the cross sections of the volume \mathcal{V} . With $S_L/S_M \sim 0.011$ and $\eta_0 = 0.23$ in our current experiment, an efficiency of $\eta = 0.25\%$ is reached. A much larger efficiency of the order of η_0 becomes accessible in an optimized geometrical setup where the microwave field M propagates collinearly with the optical fields such that $S_L/S_M \sim 1$. This is consistent with the efficiency achieved with a similar near-resonance frequency mixing scheme in the optical domain [23].

In conclusion, we have demonstrated coherent microwave-to-optical conversion in free space via a six-wave mixing process involving cold Rydberg atoms. The experimental data are in excellent agreement with a theory based on single-atom physics for the description of the interaction between the atomic medium and the electromagnetic fields. This result supports the feasibility of the conversion scheme based on Rydberg atoms proposed in [18] where near-unity efficiency can be reached. In practice, such converters will require good mode-matching between the microwave fields and the auxiliary optical fields, which can be fulfilled either by tightly

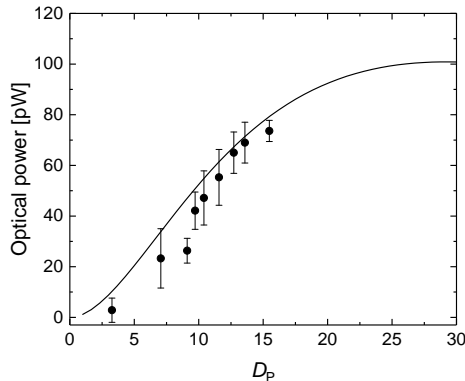


FIG. 3. **Dependence on optical depth.** The power of the converted light field L is measured for different optical depths D_P . All fields are on resonance, and the experimental parameters are given in the Methods. The black circles are experimental data, while the solid line is the corresponding theoretically simulated curve. The displayed error bars correspond to a statistical confidence interval of 1σ .

focusing the microwave or THZ radiation, or by confining it to a waveguide directly coupled to the conversion medium [11, 27].

METHODS

Atomic sample preparation and experimental cycle.

The preparation of the atomic cloud starts with loading a magneto-optical trap (MOT) and is followed by standard sub-Doppler cooling that reduces the temperature to about $20(5) \mu\text{K}$ (see Ref. [28] for details). A downwards pointing bias magnetic field of $6.1(1) \text{ G}$ is then applied to define the quantization axis z . After 2.5 ms of time-of-flight (TOF), which ensures a sufficiently stable bias field, atoms are then optically pumped into the $|5S_{1/2}, F=2, m_F=2\rangle$ state. During this stage, a variable fraction of the atoms is de-pumped into the $|5S_{1/2}, F=1\rangle$ level, which allows us to control the population in the $|5S_{1/2}, F=2, m_F=2\rangle$ state, therefore the optical depth, without changing the atomic cloud size. Finally, after another 5 ms TOF, all the input laser and microwave fields for the conversion experiment are switched on simultaneously. The atomic cloud prepared this way has a $1/e^2$ radius of $w_z = 1.6(1) \text{ mm}$ and an optical depth of $D_P = 13.7(5)$ for the data presented in Figs. 1 and 2, and $w_z = 1.8(1) \text{ mm}$ and varied D_P for the data in Fig. 3. Here the optical depth D_P is defined for the field driving the $|1\rangle \leftrightarrow |2\rangle$ transition, and its calibration is detailed in the Supplementary Information.

Laser setup.

The light for the P field is generated by a commercial 780 nm laser (Toptica DL PRO 100). The beams for both C and R fields are derived from the same 480 nm frequency-doubled diode laser system (Toptica TA-SHG pro) and are then frequency shifted separately by means of acousto-optic modulators (AOMs). These two lasers are frequency locked to a single high-finesse temperature stabilized Fabry-Perot cav-

ity, which results in a linewidth of below 20 kHz for each laser. The polarizations of the P, C, and R fields are set to be σ^+ , σ^- , and σ^+ , respectively. The beam waists of the P, C, and R fields at the center of the Gaussian atomic cloud are $w_P = 25 \pm 1 \mu\text{m}$, $w_C = 61 \pm 1 \mu\text{m}$, and $w_R = 47 \pm 1 \mu\text{m}$; their corresponding Rabi frequencies at the centers of the Gaussian beam waists are $\Omega_P^{(0)} = 1.12(3) \text{ MHz}$, $\Omega_C^{(0)} = 8.4(5) \text{ MHz}$, and $\Omega_R^{(0)} = 6.0(5) \text{ MHz}$, respectively. The calibrations of the Rabi frequencies and the beam waists are detailed in the Supplementary Information as well as in Ref. [28].

Microwave setup.

The two microwave fields are generated by two different microwave sources. The M field is obtained by frequency tripling the signal from a 20 GHz microwave synthesizer (Keysight N5183B) via a passive tripler, while the A field is generated by successive multiplication of the signal from a 6 GHz synthesizer (SRS SG386), first with an active frequency doubler and then with an active multiplier chain $\times 8$. The two microwave fields, both π polarized and enclosing an angle of 35° between their wave vectors, radiate out of two separate horn antennas and propagate in the horizontal plane through the center of the atomic cloud. The two gain horns are placed about 20 cm away from the atomic cloud, and the microwave fields pass through a vacuum view port to reach the atomic cloud. Therefore the Rabi frequencies Ω_M and Ω_A are approximately uniform across the atomic cloud volume that intersects with the laser beams. The Rabi frequencies of the A and M fields are $\Omega_A = 1.25(10) \text{ MHz}$, $\Omega_M = 1.3(1) \text{ MHz}$ for Figs. 1 and 3 and varied Ω_M for Fig. 2. The details of the microwave Rabi frequency calibrations are presented in the Supplementary Information.

Measurement and data acquisition.

The P and L fields that emerge from the atomic cloud are collected by a diffraction-limited optical system (see Ref. [28] for details). The two beams of opposite circular polarizations are separated using a quarter-wave plate and a polarization beam splitter (PBS). The powers of the two fields are then measured with two avalanche photodiode detectors, Hamamatsu C12073 and Hamamatsu C12073-01, respectively. The overall sensitivity of the detection is $9.4(5) \times 10^6 \text{ V/W}$ for the P field, and $66(3) \times 10^6 \text{ V/W}$ for the L field, respectively. The rise time of the Hamamatsu C12073-01 detector is of the order of $4 \pm 1 \mu\text{s}$. Each optical power measurement is an average of the recorded time-dependent signal in the range from 6 to $16 \mu\text{s}$ after switching on all the fields simultaneously, where the delay ensures the steady state is fully reached. Each data point is an average of 4-25 measurements.

For the beat measurement between the P field and the L field exiting from the atomic cloud, the optical frequency of the P field is shifted by means of an AOM before overlapping with the L field, so that the beat frequency falls within the bandwidth of the detector. The spectrum is obtained by Fourier transforming the recorded time-dependent beat note over $500 \mu\text{s}$.

Theoretical model.

We model the interaction of the laser and microwave fields with the atomic ensemble within the standard framework of coupled Maxwell-Bloch equations. The time evolution of the atomic density operator is modelled by a Markovian master equation,

$$\partial_t \varrho = -\frac{i}{\hbar} [H, \varrho] + \mathcal{L}_\gamma \varrho + \mathcal{L}_{\text{deph}} \varrho, \quad (1)$$

where H is the Hamiltonian describing the interaction of a

single atom with the six fields. The term $\mathcal{L}_{\gamma\rho}$ in Eq. (1) accounts for spontaneous emission of the excited states. These processes are described by standard Lindblad decay terms. The last term in Eq. (1) accounts for dephasing of atomic coherences due to finite laser linewidths, atomic collisions and dipole-dipole interactions between Rydberg atoms.

We only treat fields P and L in a self-consistent way and assume that the depletion of the other fields is small. The propagation of the P and L fields inside the medium is governed by Maxwell's equations. In the paraxial approximation we find

$$\left(-\frac{i}{2k_P}\Delta_{\perp} + \frac{1}{c}\partial_t + \partial_z\right)\Omega_P = 2i\eta_P\rho_{21}, \quad (2a)$$

$$\left(-\frac{i}{2k_L}\Delta_{\perp} + \frac{1}{c}\partial_t + \partial_z\right)\Omega_L = 2i\eta_L\rho_{61}, \quad (2b)$$

where k_P (k_L) is the wavenumber of the P (L) field, $\Delta_{\perp} = \partial_x^2 + \partial_y^2$ is the transverse Laplace operator and $\eta_{M,L}$ are coupling constants. The set of equations (1) and (2) represent a system of coupled, partial differential equations and have to be solved consistently for given initial and boundary conditions. We numerically find the steady-state solution of Eqs. (1) and (2) with MATHEMATICA [29] and the implicit differential-algebraic solver (IDA) method option for NDSolve.

The theoretical model contains one free fit parameter, which is the dephasing rate γ_{DD} due to dipole-dipole interactions on the $|4\rangle \leftrightarrow |3\rangle$ and $|4\rangle \leftrightarrow |5\rangle$ transitions. We determine its value from a fit to the transmitted spectrum of the P field in Fig. 1c, as described in the Supplementary Information, and the value of γ_{DD} is kept fixed for all other simulations. All remaining parameters used in simulations are taken from experimental measurements and calibrations and are provided in the Supplementary Information, where we also present a more detailed derivation of our model.

[1] Adam, A. J. L. Review of near-field terahertz measurement methods and their applications. *J. Infrared Milli. Terahz. Waves* **32**, 976-1019 (2011).
[2] Chan, W. L., Deibel, J. and Mittleman, D. M. Imaging with terahertz radiation. *Rep. Prog. in Phys.* **70**, 1325-1379 (2007).
[3] Tonouchi, M. Cutting-edge terahertz technology. *Nature Photon.* **1**, 97-105 (2007).
[4] Zhang, X. C., Shkurinov, A., and Zhang, Y. Extreme terahertz science. *Nature Photon.* **11**, 16-18 (2017).
[5] Xiang, Z.-L., Ashhab, S., You, J. Q., and Nori, F. Hybrid quantum circuits: Superconducting circuits interacting with other quantum systems. *Rev. Mod. Phys.* **85**, 623-653 (2013).
[6] Kimble, H. J. The quantum internet. *Nature* **453**, 1023-1030 (2008).
[7] Hisatomi, R., Osada, A., Tabuchi, Y., Ishikawa, T., Noguchi, A., Yamazaki, R., Usami, K., and Nakamura, Y. Bidirectional conversion between microwave and light via ferromagnetic magnons. *Phys. Rev. B* **93**, 174427 (2016).
[8] Williamson, L. A., Chen, Y.-H., and Longdell, J. J. Magneto-optic modulator with unit quantum efficiency. *Phys. Rev. Lett.* **113**, 203601 (2014).

[9] O'Brien, C., Lauk, N., Blum, S., Morigi, G., and Fleischhauer, M. Interfacing superconducting qubits and telecom photons via a rare-earth-doped crystal. *Phys. Rev. Lett.* **113**, 063603 (2014).
[10] Blum, S., O'Brien, C., Lauk, N., Bushev, P., Fleischhauer, M., and Morigi, G. Interfacing microwave qubits and optical photons via spin ensembles. *Phys. Rev. A* **91**, 033834 (2015).
[11] Hafezi, M., Kim, Z., Rolston, S., Orozco, L., Lev, B., and Taylor, J. Atomic interface between microwave and optical photons. *Phys. Rev. A* **85**, 020302 (2012).
[12] Strekalov, D. V., Schwefel, H. G. L., Savchenkov, A. A., Matsko, A. B., Wang, L. J., Yu, N. Microwave whispering-gallery resonator for efficient optical up-conversion. *Phys. Rev. A* **80**, 033810 (2009).
[13] Rueda, A., Sedlmeir, F., Collodo, M. C., Vogl, U., Stiller, B., Schunk, G., Strekalov, D. V., Marquardt, C., Fink, J. M., Painter, O., Leuchs, G., and Schwefel, H. G. L. Efficient microwave to optical photon conversion: an electro-optical realization. *Optica* **3**, 597-604 (2016).
[14] Bochmann, J., Vainsencher, A., Awschalom, D. D., and Cleland, A. N. Nanomechanical coupling between microwave and optical photons. *Nature Phys.* **9**, 712-716 (2013).
[15] Andrews, R., Peterson, R., Purdy, T., Cicak, K., Simmonds, R., Regal, C., and Lehnert, K. Bidirectional and efficient conversion between microwave and optical light. *Nature Phys.* **10**, 321-326 (2014).
[16] Bagci, T., Simonsen, A., Schmid, S., Villanueva, L. G., Zeuthen, E., Appel, J., Taylor, J. M., Sørensen, A., Usami, K., Schliesser, A., and Polzik, E. S. Optical detection of radio waves through a nanomechanical transducer. *Nature* **507**, 81-85 (2014).
[17] Wade, C. G., Šibalić, N., de Melo, N. R., Kondo, J. M., Adams, C. S., and Weatherill, K. J. Real-time near-field terahertz imaging with atomic optical fluorescence. *Nature Photon.* **11**, 40-42 (2016).
[18] Kiffner, M., Feizpour, A., Kaczmarek, K. T., Jaksch, D., and Nunn, J. Two-way interconversion of millimeter-wave and optical fields in Rydberg gases. *New J. Phys.* **18**, 093030 (2016).
[19] Gallagher, T. F. *Rydberg Atoms*. Cambridge University Press, 1994.
[20] Mohapatra, A. K., Jackson, T. R., and Adams, C. S. Coherent optical detection of highly excited Rydberg states using electromagnetically induced transparency. *Phys. Rev. Lett.* **98**, 113003 (2007).
[21] Fleischhauer, M., Imamoglu, A., and Marangos, J. P. Electromagnetically induced transparency: Optics in coherent media. *Rev. Mod. Phys.* **77**, 633-673 (2005).
[22] Merriam, A. J., Sharpe, S. J., Xia, H., Manuszak, D., Yin, G. Y., and Harris, S. E. Efficient gas-phase generation of coherent vacuum ultraviolet radiation. *Opt. Lett.* **24**, 625-627 (1999).
[23] Merriam, A. J., Sharpe, S. J., Shverdin, M., Manuszak, D., Yin, G. Y., and Harris, S. E. Efficient nonlinear frequency conversion in an all-resonant double- λ system. *Phys. Rev. Lett.* **84**, 5308 (2000).
[24] Harris, S. E. Electromagnetically induced transparency with matched pulses. *Phys. Rev. Lett.* **70**, 552-555 (1993).
[25] Harris, S. E. Normal modes for electromagnetically transparency. *Phys. Rev. Lett.* **72**, 52 (1994).
[26] Arimondo, E. in *Progress in Optics* (ed. Wolf, E.) Vol.

- 35, 257-354, Ch. 5 (Elsevier, Amsterdam, 1996).
- [27] Hogan, S. D., Agner, J. A., Merkt, F., Thiele, T., Filipp, S., and Wallraff, A. Driving Rydberg-Rydberg transitions from a coplanar microwave waveguide. *Phys. Rev. Lett.* **108**, 063004 (2012).
 - [28] Han, J., Vogt, T., Manjappa, M., Guo, R., Kiffner, M., and Li, W. Lensing effect of electromagnetically induced transparency involving a Rydberg state. *Phys. Rev. A* **92**, 063824 (2015).
 - [29] Wolfram Research, Inc., *Mathematica Version 10.1*. Irvine: Wolfram Research, Inc., Champaign, Illinois.

ACKNOWLEDGMENTS

The authors acknowledge the support by the National Research Foundation, Prime Ministers Office, Singapore and the Ministry of Education, Singapore under the Research Centres of Excellence programme. This work is supported by Singapore Ministry of Education Academic Research Fund Tier 2 (Grant No. MOE2015-T2-1-085). M.K. would like to acknowledge the use of the University of Oxford Advanced Research Computing (ARC) facility in carrying out this work (<http://dx.doi.org/10.5281/zenodo.22558>).